Audio Engineering Society

Convention Paper 10359

Presented at the 148th Convention, Online
2020 June 2-5

Non-linear acoustic losses prediction in vented loudspeaker using computational fluid dynamic simulation

Yves Pene[1], Yoachim Horyn[1], and Christophe Combet[1]

[1] *L-Acoustics, 13 rue Levacher Cintrat, 91460 Marcoussis, France.*

Correspondence should be addressed to Yves Pene (yves.pene@l-acoustics.com)

ABSTRACT

Bass-reflex designs can exhibit strong non-linear behaviour around their resonant frequency with significant acoustic losses and parasite noise emission. These phenomena are mainly due to turbulences and flow separation at the port's inlet and outlet. This work proposes a method to predict the resulting non-linear acoustic losses for a given loudspeaker, enclosure volume and port geometry. The approach consists of coupling computational fluid dynamics (CFD) simulation with loudspeaker non-linear motion modelization. Four different ports geometries mounted on one given loudspeaker enclosure are tested. The computed acoustic losses are compared with measurements and show a good agreement. The obtained results prove that the proposed method can predict non-linear losses with an average error less than 1 dB around the Helmholtz frequency.

1 INTRODUCTION

1.1 The bass reflex port

The bass reflex design is one of the most used approach when an engineer wants to increase the SPL over a certain low frequency range of a system without increasing the enclosure's volume. The bass reflex works on the principle of adding a Helmholtz resonator to the loudspeaker enclosure. This resonator consists of a vented port connected to the internal air volume of the enclosure and the external air volume. The resonant frequency of a variable cross section port is given by the following formula [1],

$$f_H = \frac{c}{2\pi}\sqrt{\frac{S_0}{L_{eff}V}}, \qquad (1.a)$$

where S_0 and V are respectively a reference cross-sectional area of the port section and the enclosure volume. L_{eff} is the effective length of the port such as,

$$L_{eff} = \int_0^L \frac{S_0}{S(x)}dx, \qquad (1.b)$$

where L is the physical length of the port and $S(x)$ its cross-sectional area at axial coordinate x . In practice we can add an end correction to L_{eff} to consider the mass of air moving in front of the port output [2].

It is well known that around the resonant frequency, vented ports can exhibit strong non-linear behaviour [3]. Several experimental studies conducted in the 1950s have pointed out that non-linearities in Helmholtz resonator found their origins in complex fluid phenomena such as turbulent boundary layer and vortex shedding [2]. These effects were later observed in typical vented box designs, and identified as the cause for significant acoustic loss, generation of distortion and emission of broadband noise [3][4][5]. Roozen *et al.* [1] have demonstrated that most of these phenomena are observed when the periodic displacement of the air in the port is large

compared to the dimension of the port itself, *i.e.* when the velocity gradient along the port section is important. Consequently, these issues are proportional with the driving voltage and generally become audible only at high level for a decent bass reflex design [6].

1.2 Theoretical approach

When the flow reaches the output of the port, an adverse pressure gradient occurs. The static pressure p increases in the direction x of the flow such as $\frac{\partial p}{\partial x} > 0$, leading to a significant deceleration. This phenomenon may cause a change in the sign of the velocity vector where its values are low, and especially near the wall due to the no slip condition [4]. The consequence is the appearance of flow separation and vortex shedding as illustrated on Fig. 1.

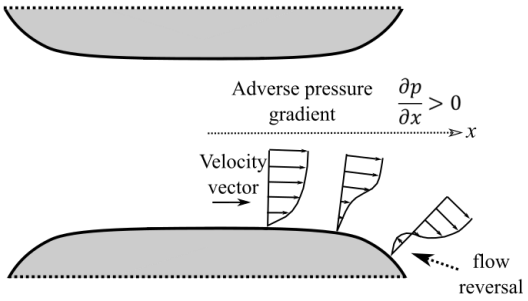

Fig. 1: Illustration of the flow reversal inside a vent port due to an adverse pressure gradient.

This fluid mechanics problem can be modelled by Navier-Stokes equations, which are presented below in the incompressible and dimensionless form,

$$\partial_t \boldsymbol{V} + (\boldsymbol{V}.\nabla)\boldsymbol{V} = -\frac{1}{\rho}\nabla P + \frac{1}{Re}\Delta \boldsymbol{V}, \qquad (2)$$

$$\text{with } Re = \frac{UD}{\nu}.$$

Re is the Reynolds number. U and D are scales associated respectively with the velocity and the characteristic dimensions of the flow, which in our case is the smallest of the dimensions between the diameter and the length of the port. ν is the kinematic viscosity of the considered fluid. P and $\boldsymbol{V}$ are respectively the dimensionless pressure and velocity field. $-\nabla P$ stands for the normal constrains associated with the pressure force, $(1/Re)\Delta \boldsymbol{V}$ is a linear diffusion term corresponding to the viscous forces. $(\boldsymbol{V}.\nabla)\boldsymbol{V}$ is a non-linear convective term with a quadratic dependency to the velocity that is related to the inertial forces.

In laminar flow regime Re is low (typically $Re << 1$) and the non-linear term $(\boldsymbol{V}.\nabla)\boldsymbol{V}$ is dominated by the linear term $(1/Re)\Delta \boldsymbol{V}$. The acoustic losses in the vent are essentially related to viscous friction effects that are linear with the air velocity in the port. This phenomenon is generally described by a resistance in the classical lumped parameters transducer modelization.

For $Re >> 1$, the equations are dominated by the non-linear convective term $(\boldsymbol{V}.\nabla)\boldsymbol{V}$. The shear stresses caused by the velocity gradient become too important and can no longer balance the viscous friction effects. A part of the acoustical energy is then transformed into rotational kinetic energy by the mean of vortex shedding [7], see Fig. 2.

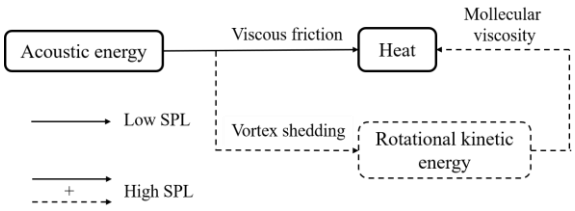

Fig. 2: Illustration of the acoustic energy dissipation in a vent port.

This phenomenon corresponds to the non-linear part of the loss that is generally not modelled in electro-acoustic simulation. The higher the Reynolds number, the more complex and turbulent the flow. For the specific case of oscillating flows, the turbulent behaviour can be predicted more precisely using the dimensionless Strouhal number defined as,

$$St = \frac{\omega D}{U}, \qquad (3)$$

where ω is the angular frequency. As described by Roozen *et al.* [1], a number $St \leq 1$ will lead to flow separation and vortices formation. More generally, for a given Helmholtz frequency f_H and enclosure's volume V, a smaller section S_0 leads to higher velocity magnitude in the vent [8]. Consequently, the Strouhal number is higher, and the losses are more likely to become significant as the driving voltage increases. Roozen *et al.* [1] showed that a bass-reflex system tuned at $f_H = 50$ Hz with a straight cylindrical port of radius 1 cm may be subjected to vortex shedding for a sound pressure level of 60 dB at one-meter distance.

With the rise of computational fluid dynamics (CFD) software solutions, several authors have attempted to simulate the flow in the vent ports in order to optimize their shapes [5][1]. Some authors have also tried to simulate simultaneously the flow and the acoustic response of the vent [9].

More recently Garcia *et al.* [10] have proposed to compute fluid equations, including acoustic phenomena, in the full enclosure volume with the vent and the exterior air domain. The loudspeaker was modelled by a planar piston with no coupling with its surrounding air volume. They have been able to reproduce emergence of turbulence and the associated broadband noise. Backman [11] proposed the same type of simulation with the addition of a more realistic loudspeaker modelization. It is modelized by impedance sources having realistic Thiele & Small parameters. The obtained results are quite promising and show non-linear effects appear such as acoustic loss and resonant frequency shift. However, the approach needs to be quantitively assessed with experimental comparison of acoustic responses.

In the aeroacoustics field, several authors have shown that implementation of CFD simulation was able to predict quantitatively precise non-linear absorption of Helmholtz resonator with Strouhal number similar to those typically found in a bass reflex port [12].

1.3 Work objective

The objective of this work is to develop a simulation method capable of predicting non-linear acoustic loss in vented port systems. The simulation is based on the Thiele & Small parameters of the loudspeaker and on the enclosure's three-dimensional geometry. In order to assess the approach, the obtained results are confronted to experimental measurements. In the first part, the different methods used to simulate the complex fluid behaviour and loudspeaker movements are presented. In the second part we detail the different test cases and the experimental protocols used to measure the acoustic losses. Finally, numerical and experimental results are compared and discussed.

2 SIMULATION METHODOLOGY

The finite element simulation software COMSOL Multiphysics © is chosen to compute the whole problem. The multiphysics approach is particularly needed to represent a loudspeaker enclosure, which is subject to strong electrical and mechanical coupling. Due to the non-stationarity of the problem, the simulation is computed in the time domain. The loudspeaker is considered as a circuit with lumped parameters. It is classically described by the following coupled differential equations [13]:

$$U(t) = R_E i(t) + BL(x)v(t) + L_E(x)\frac{di}{dt}, \quad (4)$$

$$BL(x)i(t) = M_{ms}\frac{dv}{dt} + R_{ms}v(t) + k_{ms}(x)x(t) + F_A(t) \quad (5)$$

where M_{ms}, R_{ms}, $v(t)$, $x(t)$ are respectively the mobile mass, the mechanical resistance, the velocity and the displacement of the driver and where R_E, $U(t)$, $i(t)$ are the electrical resistance, the applied voltage and the current. $F_A(t)$ corresponds to the pressure force applied by the air on the two faces of the driver. Finally, $L_E(x)$, $BL(x)$, $k_{ms}(x)$ are the

inductance, the force factor and the stiffness of the loudspeaker. These three parameters depend on the membrane displacement x. Thus, Eq. (4) and Eq. (5) are non-linear differential equations.

As proposed by Klippel [13], it is possible to make the resolution of these equations easier by rearranging them into a state variable model. In consequence, the system computed in the simulation software is given by,

$$\begin{aligned} &\frac{dx}{dt} - v = 0, \\ &\frac{1}{M_{ms}}(BL(x)i(t) - k_{ms}(x)x(t) - R_{ms}v(t) \\ &- F_A(t)) - \frac{dv}{dt} = 0, \\ &\frac{1}{L_E(x)}\big(U(t) - R_E i(t) - BL(x)v(t)\big) - \frac{di}{dt} = 0, \end{aligned} \tag{6}$$

where $[x, v, i]^T$ is the state vector of the model. One then focuses on the simulation of air behaviour in domains where non-linear fluid effects occur as turbulence and flow separation. The concerned areas are the enclosure and the port's volume but also the exterior air volume surrounding the system. It has been shown, in Helmholtz resonator, that viscous forces play a much more important part than thermal conduction regarding the diffusion induced dissipation [2]. Consequently, the air volume is considered isothermal in order to reduce the complexity of the simulation.

It is also necessary to consider this air volume compressible in order to make the propagation of acoustic waves possible. The last important assumption is the non-stationarity of the problem due to the oscillating nature of the studied phenomena. Considering all these aspects, it is chosen to use the compressible LES (Large Eddy Simulation) approach. LES method consists in simulating the full Navier-Stokes equations by filtering the smallest eddies, which are replaced by an analytical model of turbulence. This type of method has proven to be reliable for simulation of non-stationary fluid flow at high Reynolds number with lower computational cost than Direct Numerical Simulation (full simulation of Navier-Stokes equations).

The loudspeaker displacement $x(t)$, which is fully coupled with LES simulated air pressure $F_A(t)$, see Eq. (5), is applied via a moving wall condition. At a certain distance of the port output, where the potential eddies are damped, the only remaining perturbations considered are the propagating acoustic waves. Thus, the air inside the concerned domain is modeled by more classical acoustic wave equation. The "LES domain" and "Acoustic domain" are coupled in order to ensure propagation of acoustic waves. Non-reflective conditions are considered using perfectly matched layers at the external boundary of the "Acoustic domain".

3 EXPERIMENTAL TEST CASE

3.1 Setup description

The experimental enclosure has been conceived in order to have replaceable vented ports while ensuring constant volume. Its shape is rectangular, and all the dimensions are summarized on Fig. 3.

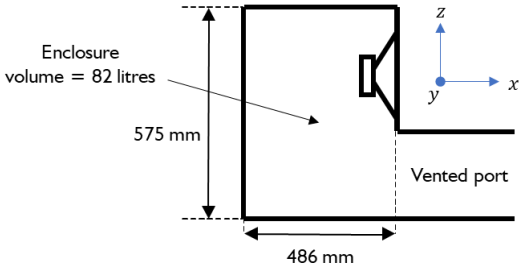

Fig. 3: Schematics of the experimental enclosure with vented port.

Four different vented ports have been designed with simulation tools in order to ensure a resonance frequency $f_H = 42$ Hz with the enclosure. The first three have cylindrical shapes with different lengths

and sections. The last one has a horizontal flare in order to reduce the amount of turbulence. The four vent ports are schematized Fig. 4, and their respective computed Strouhal number St are listed in Tab.1. Finally, the loudspeaker has been chosen with a strong force factor in order to have the maximum sensitivity at the resonant frequency f_H.

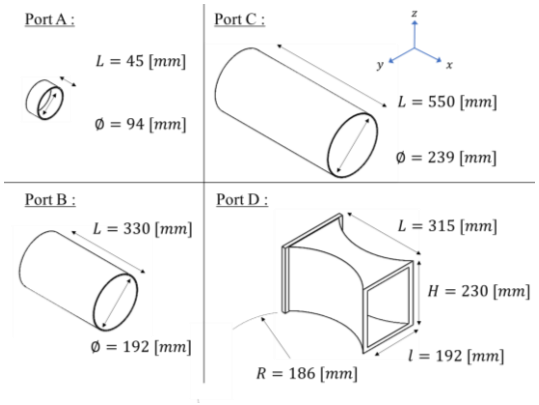

Fig. 4: Schematics of the removable vented ports. L, l, Ø, H and R are respectively the length, the width, the diameter, the height and the curvature radius of the ports.

	Port A	Port B	Port C	Port D
St	0.24	1.80	3.71	0.55

Table 1. Strouhal number evaluated by simulation with $V_{rms} = 70\ V$ for the different vented ports.

3.2 Measuring bench

In order to be able to validate the results obtained with simulations, it is necessary to conduct experimental measurements. First the loudspeaker is mounted on an infinite baffle and its displacement is measured with laser vibrometer linked to a Klippel R&D System ©. This procedure allows to measure the loudspeaker parameters M_{ms} , R_{ms} , R_E and also $L_E(x)$, $BL(x)$, $k_{ms}(x)$ as a function of the displacement x. The loudspeaker is then mounted in the enclosure with different vented ports. In order to quantify the potential impact of experimental conditions, measurements are performed outdoors and indoors. Indoor tests are carried out in a large room ($\sim 1600\ m^3$) with a third of its surface acoustically treated. This non anechoic room offers low noise-to-signal ratio and stable temperatures. Outdoor measurements are performed in a relatively open field with few reflective objects nearby, see Fig. 5. However, noise to signal ratio is not negligible and temperatures can evolve quickly in function of sun exposure. For both cases, the measurements system consists in a microphone positioned at 3.16 meters distance of the vent output.

Fig. 5: Outdoor measurement setup for acoustic loss measurement.

The loudspeaker is powered by an amplifier without equalization and a rail voltage at least 3 dB higher than those used in this work. The microphone and the amplifier are linked to a soundcard allowing to simultaneously send the test signal to the amplifier and record the microphone signal. To obtain the acoustic loss of each configuration, low and high levels measurements and simulations are both computed at $V_{rms} = 7\ V$ and $V_{rms} = 70\ V$. In order to get more points of comparison, port A is also computed at $V_{rms} = 14.0$, 27.9 and $44.2\ V$. All measurements are performed at the octave of interest ranging from 30 to 60 Hz.

4 SIMULATION VALIDATION

4.1 Simulation conditions

The sweep source signal used for the simulation ranges from 20 to 60 Hz with a peak amplitude of $\sqrt{2} * V_{rms}$ and a total duration of $t = 0.2$ s. The frequency range is extended compared to

measurements in order to ensure numerical convergence at 30 Hz. Only half of the problem is computed thanks to the width symmetry of the studied geometries. The average simulation time needed for each configuration is 8 hours on a standard computer unit (Intel © I7 CPU with 16 Go of RAM).

4.2 Fluid flow visualization

First, the velocity magnitude/vectors and the vorticity fields are plotted for port A respectively in Fig. 6 and Fig. 7 with $V_{rms} = 70\,V$. The fields are represented at different times of a given period T having a frequency corresponding to the Helmholtz frequency. The period is comprised between $t_1 = 0.120\,s$ and $t_2 = 0.144\,s$ such as $1\,/T = 1/(t_2 - t_1) \approx f_H$. The obtained mappings show two distinct phenomena. Velocity mapping makes vortex shedding clearly visible, especially at $t = T/3$ and $t = 4T/5$ when the air in the vent is respectively expulsed outside then sucked inside. On the other hand, vorticity mapping indicates the presence of a turbulent boundary layer along the vent wall. Despite the cylindrical symmetry of the vent port, it is important to note that the flow on the profile view is not symmetrical. The flow direction seems to be impacted by the geometry of the whole enclosure and by the initial flow condition.

The velocity and the vorticity are then plotted Fig. 8 for ports A, B, C and D at $t = T/3$ of the same period with $V_{rms} = 70\,V$, when vortex shedding and turbulent boundary layers are most noticeable. Top view is chosen, in order to observe the impact of the horizontal flare profile of port D on the flow. The maximum velocity magnitude is highest in port A with ~50 m/s, followed by port D with ~45 m/s, then port B and C with respectively ~20 m/s and ~18 m/s. As predicted by the port's different Strouhal number, port A exhibits the strongest vortex shedding while it is smaller for port B and port C. Things are different for port D : despite the fact that its Strouhal number is of the same order of magnitude than port A, it exhibits no vortex shedding. The flare profile allows a smoother evolution of velocity vectors at the vent output and helps to avoid flow reversal phenomenon.

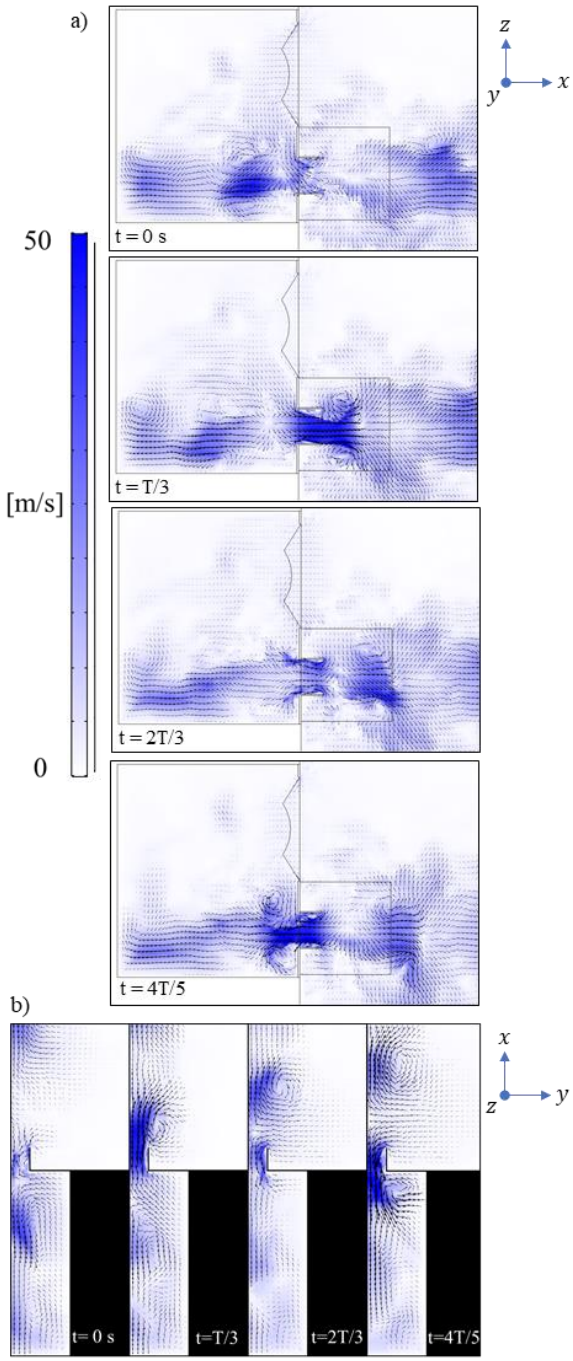

Fig. 6: Velocity magnitude at resonance for port A over one period T with $T \approx 1/f_H$ and $V_{rms} = 70\,V$: a) half port width section view; b) half port height section view.

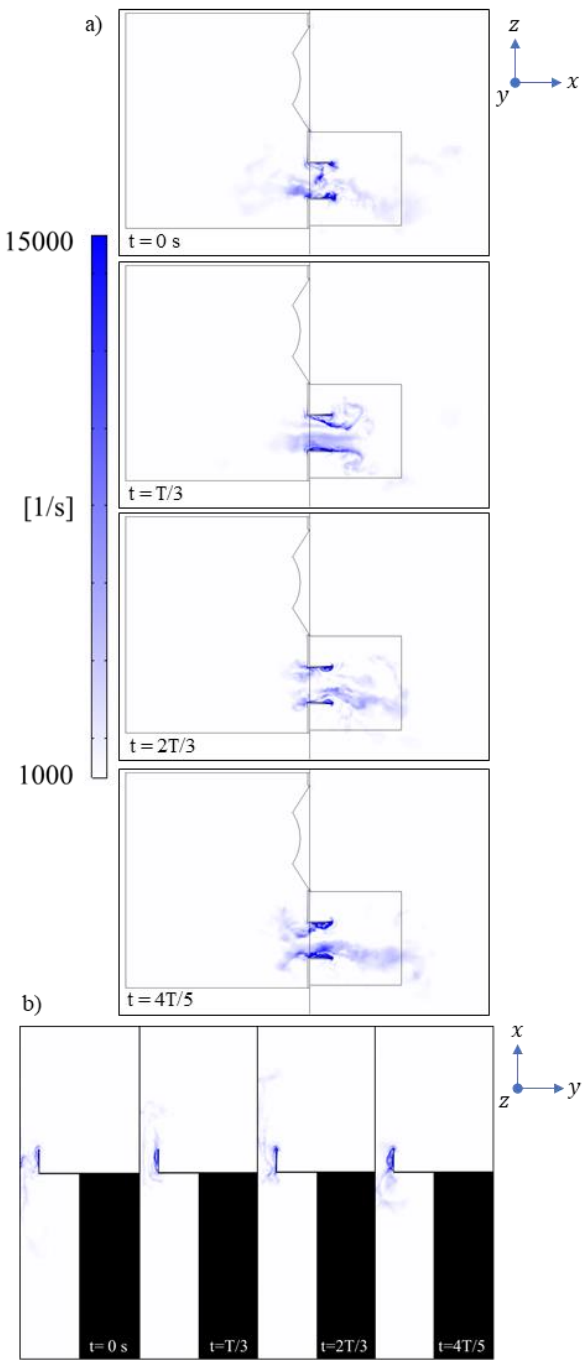

Fig. 7: Vorticity at resonance for port A over one period T with $T \approx 1/f_H$ and $V_{rms} = 70\ V$: a) half port width section view; b) half port height section view.

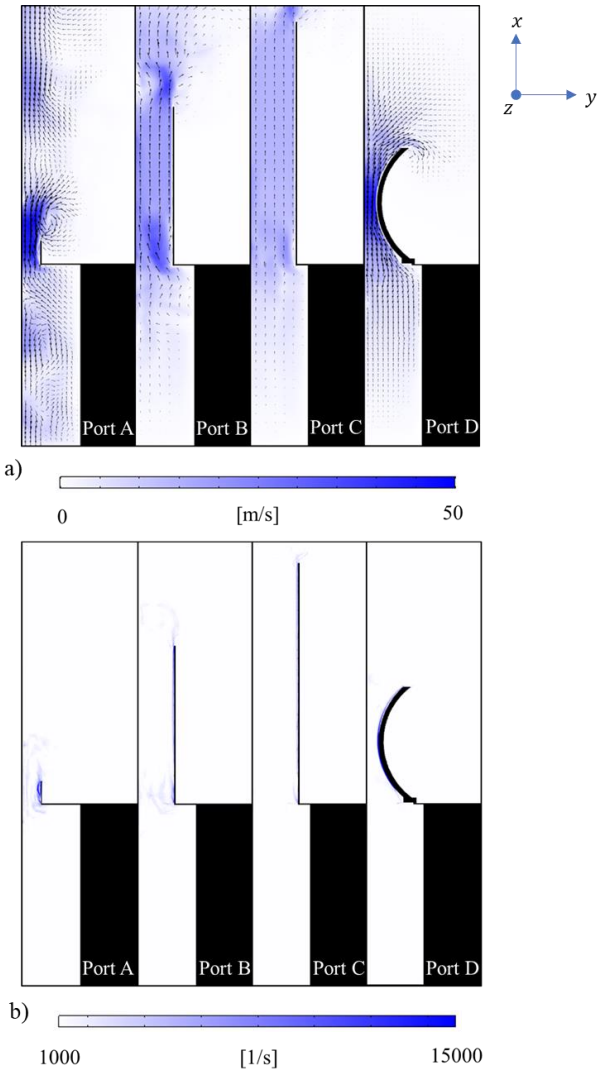

Fig. 8: Half port height section view of ports A, B, C and D at resonance for $t = T/3$ of one period T with $T \approx 1/f_H$ and with $V_{rms} = 70\ V$: a) velocity magnitude; b) vorticity.

4.3 Driver velocities

The displacement of the driver normalized by the driving voltage is then plotted for $V_{rms} = 7\ V$ and $V_{rms} = 70\ V$ and for each simulated port, see Fig. 9. On the curves of each port, one can observe three time zones that exhibit distinct behaviours.

For $t < 0.075\,s$, the simulated chirp signal evolves from $f \approx 20$ Hz to $f \approx 35$ Hz. The driver displacement is maximal and on opposite phase with the air inside the vent port. In this zone one can observe strong saturation on signal at $V_{rms} = 70\,V$, which means that strong non-linearities occur. Except for a few differences, the plotted curves are identical for each port tested. This suggests that these non-linearities are more related to the driver behaviour and that air velocities inside the vent port are relatively slow.

Between $t \approx 0.075\,s$ and $t \approx 0.150\,s$, the signals evolve from $f \approx 35$ Hz to $f \approx 50$ Hz which is around $f_H = 42\,Hz$. The driver displacements are minimal as the air velocities in the ports are maximal. One observes strong amplitude differences between each port for $V_{rms} = 7\,V$. It can also be noticed differences in non-linearities between each port by comparing $V_{rms} = 7\,V$ and $V_{rms} = 70\,V$ for all curves. This confirms that the enclosure behaviour on this band is non-linear and mostly driven by the vent port. For $t > 0.15\,s$ the signals rise from $f \approx 50$ Hz to $f \approx 60$ Hz. The driver and the vent port are in phase. At these frequencies, the normalized displacements are quite identical for each voltage and each port, suggesting a linear behaviour for both the driver and the port.

4.4 Experimental comparison of acoustic losses

In this section, the acoustic losses computed with CFD for each port are compared with experimental measurements. It is first necessary to compute the voltage normalized pressure spectrum $\overline{P_{V_{rms}}(\omega)}$ by the following formula,

$$\overline{P_{V_{rms}}(\omega)} = 20log10\left(\frac{P_{V_{rms}}(\omega)}{P_0}\right) - 20log10(V_{rms}) \quad (7)$$

where $P_{V_{rms}}(\omega)$ is the pressure spectrum at 3.16 meters from port output at V_{rms} and P_0 the atmospheric pressure. The acoustic loss $AL(\omega)$ is then given by,

$$AL(\omega) = \overline{P_{V_{rms}=70}(\omega)} - \overline{P_{V_{rms}=7}(\omega)}. \quad (8)$$

The obtained curves are plotted on Fig. 10 for the octave of interest ranging from 30 to 60 Hz. First and foremost, the measurements made outdoor are a little smoother than the indoor ones but fit well. The small oscillations on the indoor curves are potentially due to small non-linear reflexions in the room. It should also be noted that the losses around f_H are a little smaller and on the outdoor measurements with an average difference of 0.7 dB between 35 and 50 Hz and. One can also notice that the position of the maximum losses is slightly different on the three curves with respectively $f_H = 41.5,\ 40,\ 43$ Hz for indoor, outdoor and simulation.

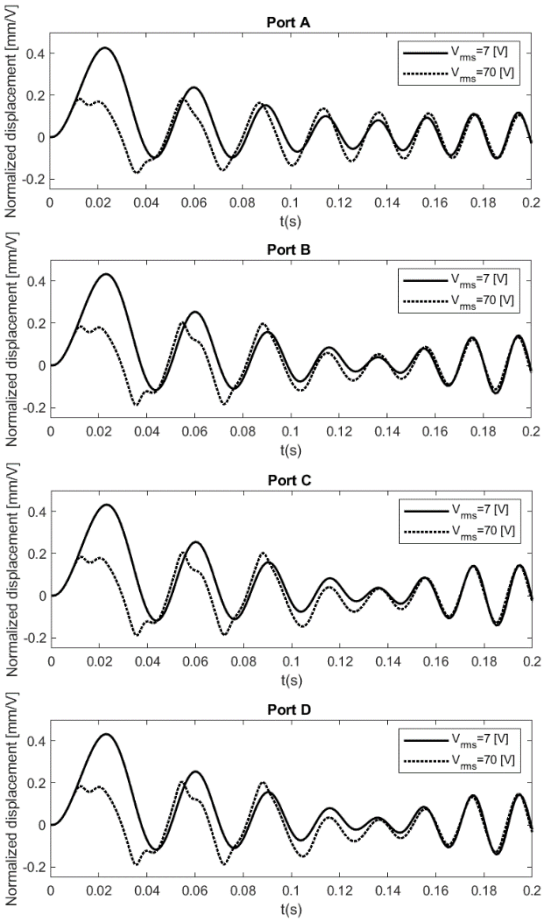

Fig. 9: Loudspeaker displacement normalized by the driving voltage for ports A, B, C and D.

Among the possible causes, this gap may potentially be due to a temperature difference of ~7 °C between the outdoor (~30 °C) and indoor (~23 °C), while simulations have been performed at 20 °C. The

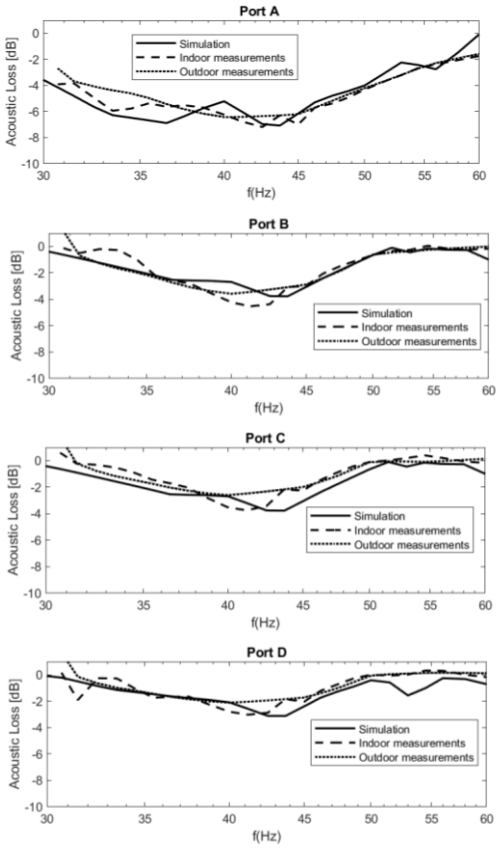

Fig. 10: Acoustic losses measured and simulated for enclosure mounted with port A, B, C and D.

temperature can have an impact on turbulent behaviour as the viscosity of a liquid decreases as temperature increases.

The second observation that can be made is the difference of experimental acoustic loss between the four ports. If we consider the indoor measurements, port A, with the lowest Strouhal number, exhibits the highest acoustic loss AL with -7 dB at f_H. As predicted by theory port B and C follow with respectively with -4.6 dB and -3.5 dB. Finally, the flared port D exhibits the lowest AL with -3.1 dB, despite the fact that its Strouhal number is lower than ports B and C. The obtained simulation curves fit well with experimental results for each port tested. The standard deviation between indoor measurements and simulation for acoustic loss are respectively 0.80, 0.72, 0.68 and 0.69 dB for ports A, B, C and D. Between outdoor measurements and simulation we obtain respectively 1.00, 0.57, 0.68 and 0.69 dB.

Fig. 11 shows computed AL for port A at $f_H = 42\ Hz$ with additional driving voltages comprised between $V_{rms} = 7\ V$ and $V_{rms} = 70\ V$. As for the preceding curves obtained, a very good agreement is found for simulation with respectively 0.24 and 0.34 dB of standard deviation with indoor and outdoor results.

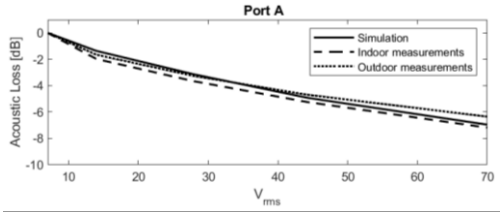

Fig. 11: Acoustic losses measured and simulated for enclosure mounted with port A at $f_H = 42\ Hz$.

To go further, the impact of temperature was investigated by performing additional simulation at 30°C for port A with $V_{rms} = 7\ V$ and $V_{rms} = 70\ V$, see Fig. 12. A maximum deviation of 0.6 dB and a standard deviation of 0.3 dB were observed on acoustic loss with the 20° simulation results, which is quite lower than the discrepancies observed with the experimental curves on the full frequency band.

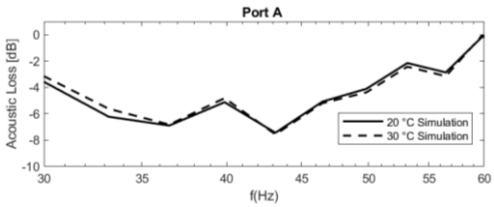

Fig. 12: Acoustic losses simulated for enclosure mounted with port A for 30°C and 20°C.

Despite the remaining differences, which can result from both environmental uncertainties and simulation hypothesis, our method is able to predict the non-linear losses around f_H with an average error less than 1 dB for the considered loudspeaker, ports and voltages.

5 CONCLUSIONS

In this work we presented a new simulation method to predict the acoustic loss in a bass reflex

loudspeaker around its Helmholtz frequency. The simulation is based on multiphysics coupling between non-linear equations of fluid motion including turbulences and acoustic phenomena and non-linear equations of the driver motion. The method has been applied to an experimental loudspeaker with removable vent ports. Four different ports with very different shapes and sizes were measured indoors and outdoors and simulated with the proposed method.

In all tested cases, the non-linear acoustic losses computed with simulation fit very well with measurements with less than 1 dB of standard deviation on octave bandwidth centered on the resonant frequency. Moreover, the obtained velocity and vorticity mapping allow to have a better insight on how turbulent boundary layers and vortex are created for a given configuration. Fluid motion mappings obtained for port A clearly show that the geometry of the enclosure can have an impact on the flow inside the vent port. It suggests that a criterion on the shape of the vent port alone may not be enough to design optimal bass reflex enclosure. Vent placement inside the enclosure, and enclosure shape should also be carefully considered, especially if low Strouhal numbers are reached.

Finally, the proposed method can help engineer to design an optimal system avoiding costly iteration steps but can also be used as a research tool to have a better insight on the complex behaviour of bass reflex enclosures. The authors would like to thank Christian Heil, Christophe Pignon and Marcel Urban who initiated the subject 15 years ago. The authors would also like to thank Hugo Coste Dombre and Vincent Baglin for their significant contributions and the staff of L-Acoustics involved in this work.

6 BIBLIOGRAPHY

[1] Roozen, N. B., Vael, J. E. M., and Nieuwendijk, J. A., “Reduction of Bass-Reflex Port Nonlinearities By Optimizing the Port Geometry,” in *Audio Engineering Society Convention 104*, Amsterdam, 1998.

[2] Ingard, U., “On the Theory and Design of Acoustic Resonators,” J. Acoust. Soc. Am. 25, 1037, 1953.

[3] Backman, J., “The Nonlinear Behaviour of Reflex Ports,” in *Audio Engineering Society Convention 98*, Paris, 1995.

[4] Salvatti, A., Devantier, A., Button, D. J. “Maximizing Performance from Loudspeaker ports,” *Journal of the Audio Engineering Society*, 50(1-2), pp. 19–45, 2002, ISSN 0004-7554.

[5] Rapoport, Z., Devantier, A., “Analysis and Modeling of the Bi-Directional Fluid Flow in Loudspeaker Ports,” in *Audio Engineering Society Convention 117*, San Francisco, 2004.

[6] Bezzola, A., Devantier, A., McMullin, E., “Loudspeaker Port Design for Optimal Performance and Listening Experience,” in *Audio Engineering Society Convention 147*, New York City, Oct 2019.

[7] Roche, J-M., Leylekian, L., Delattre G. and Vuillot, F. “Aircraft Fan Noise Absorption: DNS of the Acoustic Dissipation of Resonant Liners,” in *15th AIAA/CEAS Aeroacoustics Conference*, May 2009. Miami, Florida.

[8] Vanderkooy, J., “Loudspeaker Ports,” in *Audio Engineering Society Convention 103*, New York City, 1997.

[9] Pellerin, G., Polack, J. D. and Morkerken, J. P., “Sound source design in the very low frequency domain,” in *Audio Engineering Society Convention 116*, Berlin, May 2004.

[10] Garcia-Alcaide, V. M., Palleja-Cabre, S., Castilla, R., Gamez-Montero, P. J., Romeu, J., Pamies, T., Amate, J., and Milan, N., “Numerical study of the aerodynamics of sound sources in a bass-reflex port,” Engineering Applications of Computational Fluid Mechanics, 11(1), pp. 210–224, 2017.

[11] Backman, J., “Nonlinearity of Ported Loudspeaker enclosures”, in *Audio Engineering Society Convention 142*, Berlin, 2017.

[12] Zhang, Q., Bodony, D. J., “Numerical investigation and modelling of acoustically excited flow through a circular orifice backed by a hexagonal cavity,” J. Fluid Mech. 693, 367–401 (2012).

[13] Klippel, W., “Measurement of large-signal parameters of electrodynamic transducer,” in *Audio Engineering Society Convention* 107, 1999.